Scanning Microscopy

Volume 1992
Number 6 *Signal and Image Processing in Microscopy and Microanalysis*

Article 19

1992

Diffraction and Imaging Theory of Inelastically Scattered Electrons - A New Approach

Z. L. Wang
Oak Ridge National Laboratory, zwang@enh.nist.gov

J. Bentley
University of Tennessee

Scanning Microscopy Supplement 6, 1992 (pages 195-208) 0892-953X/92$5.00+.00
Scanning Microscopy International, Chicago (AMF O'Hare), IL 60666 USA

DIFFRACTION AND IMAGING THEORY OF INELASTICALLY SCATTERED ELECTRONS - A NEW APPROACH

Z.L. WANG*+ and J. BENTLEY

Metals and Ceramics Division, Oak Ridge National Laboratory, P.O. Box 2008
Oak Ridge, TN 37831-6376, USA

*and Department of Materials Science and Engineering, The University of Tennessee,
Knoxville, TN 37996-2200, USA

Abstract

A new dynamical theory is developed for describing inelastic electron scattering in thin crystals. Compared to existing theories, the first advantage of this new theory is that the incoherent summation of the diffracted intensities contributed by electrons after exciting vast numbers of degenerate excited states has been evaluated before any numerical calculation. The second advantage is that only the modulus squared of the transition matrix elements are needed in the final computation. This greatly reduces the effort in searching for "phase shifts" in inelastic scattering matrix calculations. By iterative operation of this single-inelastic scattering theory, multiple-inelastic electron scattering of phonons, single-electrons and valence (or plasmon) excitations can be included in diffraction pattern calculations. High resolution images formed by valence excited electrons can also be calculated in this theoretical scheme for relatively thick crystals.

The sharpness of thermal diffuse scattering (TDS) streaks is determined by the phonon dispersion relationships of the acoustic branches; optical branches contribute only a diffuse background. Dynamical scattering effects can change the intensity distribution of TDS electrons but have almost no effect on the sharpness of TDS streaks. To a good approximation, the TDS streaks are defined by the q_x - q_y curves which satisfy $\omega_j(\mathbf{q}) = 0$, where $\omega_j(\mathbf{q})$ is the phonon dispersion relationship determined by the *2-D* atomic vibrations in the (hkl) plane perpendicular to the incident beam direction $\mathbf{B}$ = [hkl] (for orthogonal crystal systems). This is a simplified 2-D vibration model. The directions of TDS streaks can be predicted according to a simple $\mathbf{q}\bullet(\mathbf{r}(\ell)-\mathbf{r}(\ell_1)) = 0$ rule, where the summation of ℓ_1 is restricted to the first nearest neighbors of the ℓ^{th} atom that are located in the same atomic plane as the ℓ^{th} atom perpendicular to the incident beam direction.

Key words: Inelastic electron diffraction, phonon excitation, single electron excitation, valence excitation, thermal diffuse scattering streaks, multiple-inelastic electron scattering, high resolution electron microscopy images of valence-loss electrons, molybdenum, silicon.

+Current address for correspondence:
Z.L. Wang
Metallurgy Division, Bldg. 223, Rm B106
National Institute of Standards and Technology
Gaithersburg MD, 20899 USA

Telephone: (301) 975-5963
FAX: (301) 926-7975
e-mail: ZWANG@ENH.NIST.GOV

Introduction

Studies of inelastic electron scattering are becoming increasingly important in developing new electron microscopy techniques and understanding the basic physical processes involved in image formation. The fundamental theory describing inelastic electron scattering in a crystal was first given by Yoshioka (1957). By considering the incident electron and the electrons in the crystal as a whole system, he derived a set of coupled Schrödinger equations that included the transitions between the ground state and the excited states of the crystal. Electron multiple-elastic and -inelastic scattering are all included in these equations. Since the life time (Björkman et al., 1967) of an excited state (typically 10^{-15} to 10^{-13} s for phonons) is much longer than the interaction time of a fast electron (100 keV) with an atom (about 10^{-18} s), the inelastic scattering of high-energy electrons can be treated as a time-independent process. Applications of this theory and other theories for single inelastic scattering have been made by many authors in various cases (Howie, 1963; Whelan, 1965a and b; Gjønnes, 1966; Gjønnes and Watanabe, 1966; Cowley and Pogany, 1968; Doyle, 1971; Humphreys and Whelan, 1969; Radi, 1970; Okamoto et al., 1971; Høier, 1973; Rez et al., 1977; Maslen and Rossouw, 1984; Rossouw and Bursill, 1985; Bird and Wright, 1989; Wang, 1989 and 1990).

The Bloch wave (Howie, 1963) and multislice theories (Wang, 1989) are the two main theoretical schemes for solving Yoshioka's coupled equations. Although, in principle, single and multiple inelastic scattering can be treated by these theories, the incoherence of different inelastic excited states makes it impractical to calculate the diffraction patterns formed by electrons that have excited the states of different energies and momenta, because the excitation of each state has to be calculated separately and added incoherently at the crystal exit face. This is a huge amount of calculation because the number of excited states tends to be infinite in practice. Thermal diffuse scattering (TDS) or phonon scattering is such an example. High energy (typically 100 keV) electrons pass through specimens so rapidly that vibrating atoms are seen as if stationary. The electron diffraction pattern and image are the sums of the intensities for the many instantaneous pictures of displaced atoms. In other words, thermal diffuse scattering is actually a statistically averaged quasi-elastic scattering (energy loss < 0.2 eV) of the electrons from the crystal with different thermal vibration configurations. Thus the final detected intensity distribution is a summation of all the possible elastic scattering from these different distorted lattices. This is the "frozen" lattice model of TDS in electron diffraction (Hall, 1965; Hall and Hirsch, 1965; Fanidis et al., 1989; Fanidis et al., 1990; Wang and Cowley, 1990; Loane et al.,1991). However, it is impractical to repeat the whole calculation for large numbers of differently distorted crystal structures. Thus an important question in simulating TDS is how to take the statistical average of the elastic electron scattering from these lattice configurations before the numerical calculations.

List of symbols

Ψ_0 = Elastic wave of energy E.
Ψ_n = Inelastic wave after exciting crystal state n.
$\mathbf{k}_n$ = Free space wave vector of energy E_n.
m_0 = Electron rest mass.
m_e = Mass of a moving electron with velocity v.
$\hbar$ = Planck's constant /2π.
H'_{nm} = Transition matrix element from state m to state n.
λ = Electron wavelength.
$\otimes$ = Convolution operation.
$V(\mathbf{r})$ = Crystal potential distribution.
$\Psi_n^0(\mathbf{r})$ = Elastic scattered wave of incident energy E_n.
$\phi_n(\mathbf{r})$ = Inelastic modulation function of $\Psi_n^0(\mathbf{r})$.
d = Crystal thickness.
$\mathbf{b}$ = Real space position (x, y).
$\hbar\mathbf{q}$ = Inelastic momentum transfer.
τ = Reciprocal space vector (τ_x,τ_y).
V_c = Volume of the unit cell.
A = Cross-section area of the unit cell perpendicular to z.
a_3 = Height of the unit cell in the z direction.
$\Delta V(\mathbf{r})$ = Deviation of crystal potential from its equilibrium state.
$V_\ell(\mathbf{r})$ = Potential of the ℓ^{th} atom.
$V'_\ell(\mathbf{r})$ = Potential of the ℓ^{th} atom including Debye-Waller factor.
$\mathbf{u}(^h_\ell)$ = Displacement of the ℓ^{th} atom in the h^{th} unit cell from its equilibrium position.
$\omega_j(\mathbf{q})$ = Phonon dispersion surface of the j^{th} phonon branch.
$\mathbf{e}(\ell\,|\,^{\mathbf{q}}_{j})$ = The ℓ^{th} atom polarization vector in the j^{th} phonon branch.
N = Total number of primitive unit cells in the crystal.
m_ℓ = Mass of the ℓ^{th} atom.
a^+ = Creation operator of a phonon.
a = Annihilation operator of a phonon.
$N(\mathbf{q},\omega)$ = Occupation number of the phonons.
T = Temperature.
k_B = Boltzman constant.
V_s = Volume of the crystal.
e = Absolute electron charge.
$\mathbf{g}$ = Reciprocal lattice vector.
$\Re$ = The Rydberg energy.
a_0 = Bohr radius.
f_{nm} = Generalized oscillator strength (GOS).
$\varepsilon(\omega,\mathbf{q})$ = Dielectric response function.
ε_0 = Dielectric constant of vacuum.
v = Electron velocity.
n_0 = Number of atoms in the primitive unit cell.
F = Interatomic force constant.
G = Interatomic force constant.
F_{OB} = Objective lens transfer function.
C_s = Objective lens spherical aberration coefficient.
Δf = Objective lens defocus.
B = The shape function of the objective aperture.
$\frac{dI_{EELS}}{d\hbar\omega}$ = Electron energy-loss intensity distribution function.
τ_c = Cut-off of momentum transfer in valence excitation.
Λ = Mean-free-path of plasmon excitation.
Δz = Thickness of a crystal slice.
Q = Phase grating function of a crystal slice.
P_n = Wave propagation function.

This problem can be solved using the newly proposed dynamical theory (Wang and Bentley, 1991a to c). The phase correlations of the localized inelastic scattering occurring at different atomic sites (in classical terms) can be statistically evaluated before any numerical calculations, essentially providing an easy way for treating coherence, incoherence or partial coherence in dynamical electron diffraction. In this paper, this new theory is reviewed and applied to treat single- and multiple-inelastic phonon, single-electron and valence excitations in electron diffraction. A comprehensive dynamical treatment of TDS is described and applied to interpret the TDS streaks observed in diffraction patterns of monoatomic f.c.c and b.c.c type of structures. Full dynamical calculations for Mo (001)will be presented. A simplified model is discussed for predicting TDS streaks without any numerical calculations. Finally, the high-resolution images formed by valence (or plasmon) excited electrons are described.

The basic theory of electron inelastic scattering

The basic equations governing inelastic electron scattering in a crystal were derived from wave mechanics (Yoshioka, 1957). If Ψ_0 describes the elastically scattered wave of energy E, and Ψ_n describes the inelastically scattered wave of energy E_n, with n=1, 2 ...., their scattering through a crystal is governed by

$$(\nabla^2 + k_n^2 - \frac{2m_e}{\hbar^2} V(\mathbf{r}))\Psi_n = \frac{2m_e}{\hbar^2} \sum_m H'_{nm}(\mathbf{r})\Psi_m, \qquad (1)$$

where H'_{nn} is is the crystal potential. By assuming electron scattering angles are of the same magnitude as Bragg angles and taking the inelastic scattering as a position modulation to an inelastic incident wave, analogous to Howie's method (1963), the solution of Eq. (1) can be written in a form

$$\Psi_n \equiv \phi_n(\mathbf{r})\, \Psi_n^0(\mathbf{r}), \qquad (2)$$

where $\Psi_n^0(\mathbf{r})$ is the elastic wave of free space wave vector $\mathbf{k}_n$, which satisfies the boundary conditions and the elastic scattering Schrödinger equation,

$$(\nabla^2 + k_n^2)\Psi_n^0 = \frac{2m_e}{\hbar^2} V(\mathbf{r})\Psi_n^0. \qquad (3)$$

It is important to point out that $\Psi_n^0(\mathbf{r})$ is the full solution of Eq. (3) rather than a single stream of a Bloch wave solution. Therefore, Eq. (2) has more general meaning than that initially defined by Howie (1963). Now one looks for the first order solution of Eq. (1). Under the small angle and forward scattering approximation, for $k_{x,y} << k_z$ (i.e., $\nabla\phi_n \bullet \nabla\Psi_n^0 \approx \partial\phi_n(\mathbf{r})/\partial z \times \partial\Psi_n^0(\mathbf{r})/\partial z$), by neglecting the $\nabla^2\phi_n$ term and using Eq. (3), Eq. (1) becomes

$$\frac{\partial\phi_n(\mathbf{r})}{\partial z} = \alpha \sum_{m\neq n} U_{nm}(\mathbf{r})\, \phi_m(\mathbf{r}), \quad \text{with n = 0, 1, 2 ...} \qquad (4a)$$

where $$U_{nm} \equiv H'_{nm}(\mathbf{r})\, \Psi_m^0(\mathbf{r}) / \frac{\partial\Psi_n^0(\mathbf{r})}{\partial z}, \qquad (4b)$$

and $\alpha \equiv \frac{m_e}{\hbar^2}$. For thin crystals satisfying $|\alpha \int_0^d dz\, U_{10}| << 1$ (i.e., $d << \frac{\lambda}{\pi}\frac{E}{H'_{10}}$), and under the single inelastic scattering approximation, for excitation state 1

$$\frac{\partial \phi_1(\mathbf{r})}{\partial z} \approx \alpha U_{10}(\mathbf{r})\phi_0(\mathbf{r}). \tag{5}$$

The boundary condition is $\phi_1(\mathbf{b},z=0) = 0$, where $\mathbf{b} = (x, y)$. If the absorption effects of the elastic wave and the multiple-inelastic scattering are neglected, by replacing symbol H'_{10} with $H'_{(1)}$, one approximately has

$$\phi_1(\mathbf{r}) \approx \alpha \int_0^z dz_1\ U_{10}(\mathbf{b},z_1), \tag{6}$$

$$\Psi_1(\mathbf{b},d) = \alpha \left\{ \int_0^d dz_1\ H'_{(1)}(\mathbf{b},z_1,\mathbf{q}) S_{(1)}(\mathbf{b},z_1) \right\} \Psi_1^0(\mathbf{b},d), \tag{7a}$$

where $$S_{(1)}(\mathbf{b},z) \equiv \Psi_0^0(\mathbf{b},z) / \frac{\partial \Psi_1^0(\mathbf{b},z)}{\partial z}. \tag{7b}$$

Equation (7) is the first order solution of Eq. (1) for thin crystals under the single inelastic scattering approximation. It has been proved that Eq. (7a) is equivalent to the inelastic scattering multislice theory proposed by several authors (Cowley and Pogany, 1968; Doyle, 1971; Wang, 1989) (see Appendix A). The multislice solution of Eq. (1) (see Eq. (A.11) in Appendix A) was derived without neglecting the $\nabla^2\phi_n$ term (Wang, 1989), therefore, this equivalence supports the validity of the approximation ($\nabla^2\phi_n\Psi_n^0 << 2\nabla\phi_n \bullet \nabla\Psi_n^0$) even for localized inelastic scattering within thin specimens.

Compared to the Bloch wave (Howie, 1963; Maslen and Rossouw, 1984) and the multislice theories, the most important feature of Eq. (7) is that the phase correlations of the inelastic scattering process occurring at different atomic sites (in classical terms) can be evaluated analytically before any numerical calculations. This provides an easy way for evaluating coherent, incoherent or partially coherent scattering between different inelastic excited states. Equation (7) has been applied to treat single phonon excitations based on the semi-classical "frozen lattice" model (Wang and Bentley, 1991a) and the full lattice dynamics (Wang, 1992a). The theoretical results have successfully interpreted the positions and intensities of the thermal diffuse streaks observed in electron diffraction patterns. Further applications of Eq. (7) have provided a simple theory that accounts for valence excitation effects in simulating high resolution electron microscopy images (Wang and Bentley, 1991b and c).

Diffraction of single inelastically scattered electrons

Phase correlations among the inelastic events (or states) critically affect the intensity distributions in diffraction patterns. Now we attempt to apply Eq. (7) for calculating the energy-filtered diffraction patterns formed by the inelastically scattered electrons. For easy notation, one replaces $\Psi_1^0(\mathbf{r})$ by $\Psi_1^0(\mathbf{r},\mathbf{q})$ to represent the inelastic incident electron wave with wave vector $\mathbf{k}$-$\mathbf{q}$. Taking a 2-D Fourier transform of Eq. (7b), in reciprocal space $\tau = (\tau_x,\tau_y)$, yields

$$\Psi_1(\tau,d) \approx \alpha \int_0^d dz\ H'_{(1)}(\tau,z,\mathbf{q}) \otimes S_{(1)}(\tau,z') \otimes \Psi_1^0(\tau,d,\mathbf{q}), \tag{8}$$

In general, for a 3-D periodic crystal structure (Howie 1963), H' can be written as,

$$H'_{(n)}(\mathbf{r},\mathbf{q}) = \exp(i\mathbf{q}\bullet\mathbf{r}) \sum_g H'^{(n)}_g(\mathbf{g}-\mathbf{q}) \exp(-i\mathbf{g}\bullet\mathbf{r}), \tag{9a}$$

or

$$H'_{(n)}(\tau,z,\mathbf{q}) = \frac{(2\pi)^2}{A} \exp(iq_z z) \sum_g H'^{(n)}_g(\mathbf{g}-\mathbf{q})\ \delta(\tau-\mathbf{g}+\mathbf{q}_b). \tag{9b}$$

Putting Eq. (9b) into Eq. (8),

$$\Psi_1(\tau,d) = \left(\frac{4\pi^2\alpha}{A}\right) \sum_g H'^{(1)}_g(\mathbf{g}-\mathbf{q})\ Z_1(\tau-\mathbf{g}+\mathbf{q}_b,q_z), \tag{10}$$

where

$$Z_1(\tau,\mathbf{q}) \equiv \left[\int_0^d dz\ \exp(iq_z z)\ S_{(1)}(\tau,z) \right] \otimes \Psi_1^0(\tau,d,\mathbf{q}). \tag{11}$$

In reciprocal space, for a finite crystal, each point represents a distinct excited state, and the different contributions at different $\mathbf{g}$ do not overlap so that a coherent superposition of the inelastic waves gives the same result as an incoherent superposition (Wang, 1989). Therefore, for diffraction pattern calculations, the interference effect between different $\mathbf{g}$'s can be neglected. Summing the intensities contributed by the inelastic scattering processes of different $\mathbf{q}$ incoherently, one obtains

$$\begin{aligned} I_1(\tau) &= \frac{V_c}{(2\pi)^3} \int_{BZ} d\mathbf{q}\ |\Psi_1(\tau,d)|^2 \\ &\approx \frac{V_c}{(2\pi)^3} \left(\frac{4\pi^2\alpha}{A}\right)^2 \sum_g \int_{BZ} d\mathbf{q}\, |H'^{(1)}_g(\mathbf{g}-\mathbf{q})|^2 \\ &\quad \times |Z_1(\tau-\mathbf{g}+\mathbf{q}_b,q_z,\mathbf{q}_1)|^2, \end{aligned} \tag{12}$$

where the integration of $\mathbf{q}$ is restricted to the first Brillioun zone (BZ); $\mathbf{q}_1$ is introduced to represent the average momentum transfer in inelastic electron scattering; and the subscript b refers to the projection of the corresponding quantity in the x-y plane. Equation (12) can be further simplified by separating the integration of $\mathbf{q}$ into $\mathbf{q}_b = (q_x, q_y)$ and q_z. By defining a function

$$T_g^{(1)}(\mathbf{g}-\mathbf{q}_b) \equiv \begin{cases} \frac{a_3}{2\pi} \int_{BZ} dq_z\, |H'^{(1)}_g(\mathbf{g}-\mathbf{q})|^2 \text{ if } \mathbf{q}_b \in \text{ the first BZ;} \\ 0, \text{ otherwise;} \end{cases} \tag{13}$$

the integration of $\mathbf{q}_b$ can thus be extended to $(-\infty,\infty)$ in reciprocal space. Since q_z is mainly related to the electron energy-loss by $q_z \approx k_0 \frac{E-E_1}{2E}$ independent of $\mathbf{q}_b$ (Egerton, 1986), to a good approximation one can take Z_1 out of the integration of q_z, and thus

$$\begin{aligned} I_1(\tau) &\approx \xi^2 \sum_g \int_{-\infty}^{\infty} d\mathbf{q}_b\, T_g^{(1)}(\mathbf{g}-\mathbf{q}_b)\ |Z_1(\tau-\mathbf{g}+\mathbf{q}_b,\mathbf{q}_1)|^2 \\ &= \xi^2\, T^{(1)}(\tau) \otimes |Z_1(\tau,\mathbf{q}_1)|^2, \end{aligned} \tag{14}$$

where $$T^{(1)} \equiv \sum_g T_g^{(1)}(\tau). \tag{15a}$$

and $$\xi = \frac{2\pi\alpha}{A^{1/2}}. \tag{15b}$$

The calculation of the Z_1 function can be performed with the multislice theory. Equation (14) can be applied to different

inelastic scattering processes, such as phonon, single-electron and valence excitations, if the corresponding T functions are known.

It is important to note that the phase shifts in inelastic scattering have been evaluated in Eq. (13) before any numerical calculation. The calculations of the T functions depend only on the modulus square of the scattering matrix element. This is a key point which makes this approach more powerful than previous ones.

Phonon scattering

Phonon scattering is generated by atomic vibrations in the crystal. Thermal vibrations introduce a small time-dependent displacement to each atom, which causes a small perturbation of the potential of the equilibrium lattice. The correction to the crystal potential due to atomic vibrations is (Takagi, 1958),

$$\Delta V(\mathbf{r}) = \sum_{h}\sum_{\ell} [V_\ell(\mathbf{r}-\mathbf{R}(h)-\mathbf{r}(\ell)-\mathbf{u}(^{h}_{\ell})) - V'_\ell(\mathbf{r}-\mathbf{R}(h)-\mathbf{r}(\ell))], \quad (16)$$

$\mathbf{u}(^{h}_{\ell})$ can be expressed as a sum of normal harmonic oscillator modes (Born, 1942; Brüesch, 1982) as,

$$\mathbf{u}(^{h}_{\ell}) = \sqrt{\frac{\hbar}{2Nm_\ell}} \sum_{\mathbf{q}}\sum_{j} \frac{1}{\sqrt{\omega_j(\mathbf{q})}} \mathbf{e}(\ell\,|\,^{\mathbf{q}}_{j}) \times \exp\{i\mathbf{q}\bullet(\mathbf{R}(h)+\mathbf{r}(\ell))\}\,[a^{+}(^{-\mathbf{q}}_{j}) + a(^{\mathbf{q}}_{j})], \quad (17)$$

where j indicates different acoustic and optical branches. For a 3-D periodic structure, the interaction Hamiltonian for creating a phonon of momentum $\mathbf{q}$ and frequency $\omega_j(\mathbf{q})$ is (Whelan, 1965a and b; Rez et al., 1977),

$$H'(\mathbf{r},\mathbf{q},\omega) = \langle N(\mathbf{q},\omega)+1\,|\,[-e\,\Delta V(\mathbf{r})]\,|\,N(\mathbf{q},\omega)\rangle \approx -i\,e\,(2\pi)^3 \sum_{\ell}\sum_{g} A_\ell(\omega_j(\mathbf{q}))\,\mathbf{e}(\ell\,|\,^{\mathbf{q}}_{j})\bullet(\mathbf{g}-\mathbf{q}) \times V_\ell(\mathbf{g}-\mathbf{q})\exp(i(\mathbf{q}-\mathbf{g})\bullet\mathbf{r})\exp(i\mathbf{g}\bullet\mathbf{r}(\ell)), \quad (18)$$

where $$V_\ell(\mathbf{g}) = \frac{1}{V_c}\int V_\ell(\mathbf{r})\,\exp(-i\mathbf{g}\bullet\mathbf{r})\,d\mathbf{r}; \quad (19)$$

$$N(\mathbf{q},\omega) = \frac{1}{\exp(\hbar\omega_j/k_BT)-1}; \quad (20a)$$

and $$A_\ell(\omega_j(\mathbf{q})) \equiv \sqrt{\frac{\hbar(N(\mathbf{q},\omega)+1)}{2\omega_j(\mathbf{q})m_\ell N}} \quad (20b)$$

is the atomic vibration amplitude in phonon mode $\omega_j(\mathbf{q})$. Thus

$$T^{(TDS)} = a_3\,e^2\,N(2\pi)^5\,\theta(\tau)\sum_{j}\sum_{\ell}\int_{BZ} dq_z\,|\,A_\ell(\omega_j(\tau)) \times(\mathbf{e}(\ell\,|\,^{\tau}_{j})\bullet\tau)\,V_\ell(\tau)\,|^2, \quad (21)$$

where sum of j is over all the phonon branches, and $\theta(\tau)$ is a "switch" function defined by

$$\theta(\tau) \equiv \begin{cases} 1 & \text{if } \tau \text{ falls within the first BZ;} \\ 0 & \text{otherwise.} \end{cases} \quad (22)$$

According to Eq. (14), the electron diffraction pattern intensity distribution from phonon single-inelastic scattering is

$$I_{TDS} = \xi^2\,T^{(TDS)}(\tau) \otimes |\,Z_1(\tau,\mathbf{q}_1)\,|^2, \quad (23)$$

The terms purely related with lattice dynamics are included in $T^{(TDS)}$, which represents the TDS intensity distribution within the first BZ and can be named the scattering power function. As will be pointed out later, the choice of $\mathbf{q}_1$ is very important for simulating TDS electron diffraction patterns. The effects related with dynamical electron scattering are contained in the Z_1 function, which is determined purely by the elastic scattering Schrödinger equation (Eq. (3)) and can be solved using the multislice method (Cowley and Moodie, 1957; Ishizuka, 1982). The "convolution" of the lattice dynamics with the electron diffraction dynamics gives the final TDS intensity distribution in the diffraction plane.

Single-electron excitations

Single-electron excitation is another important inelastic scattering process in electron diffraction, and is generated by exciting an atomic inner shell. Since this process is mainly determined by the properties of a single atom, it is possible to use the tight-binding approximation for calculating $H'_g{}^{(n)}$. Whelan (1965a) gave

$$H'_g{}^{nm} = \frac{e^2}{V_s\varepsilon_0}\frac{\varepsilon_{nm}(\mathbf{g}-\mathbf{q})}{|\mathbf{g}-\mathbf{q}|^2}, \quad (24a)$$

where $$\varepsilon_{nm}(\mathbf{K}) = \langle n|\exp(-i\mathbf{K}\bullet\mathbf{r})|m\rangle, \quad (24b)$$

$|n\rangle$ and $|m\rangle$ are the normalized one-electron atomic wave functions. If the contributions of all the atoms are considered, one obtains,

$$H'_{nm}(\mathbf{r},\mathbf{q}) = \frac{e^2}{V_c\varepsilon_0}\sum_{\mathbf{g}}\sum_{\ell}\frac{\varepsilon^{\ell}_{nm}(\mathbf{g}-\mathbf{q})}{|\mathbf{g}-\mathbf{q}|^2}\exp[i(\mathbf{q}-\mathbf{g})\bullet\mathbf{r}]\exp[i\mathbf{g}\bullet\mathbf{r}(\ell)]. \quad (25)$$

ε^{ℓ}_{nm} is related to the generalized oscillator strength (GOS) f^{ℓ}_{nm} (Inokuti, 1971) by,

$$f^{\ell}_{nm} = \frac{|E_n-E_m|}{\Re a_0^2}\frac{|\varepsilon^{\ell}_{nm}|^2}{(\tau^2+q_0^2)}, \quad (26)$$

where $q_0 \approx k_0\frac{E-E_1}{2E}$. Considering the fact that f^{ℓ}_{nm} depends weakly on τ, one can approximately take f^{ℓ}_{nm} as τ independent, thus

$$T^{(S)} \approx \left[\frac{e^2}{V_c\varepsilon_0}\right]^2\frac{N\Re a_0^2}{E-E_1}\{\sum_{\ell}|f^{\ell}_{10}|\}\left[\frac{\theta(\tau)}{\tau^2+q_0^2}\right]. \quad (27)$$

Valence excitations

Valence (or plasmon) losses are generated by collective excitations of the electrons in the crystal. These processes usually involve small energy-losses (about 10-30 eV) and small momentum transfers. Valence excitations are characterized by the dielectric response function $\varepsilon(\omega,\mathbf{q})$ of the system. According to the result of Okamoto et al. (1971), if only the g = 0 term is important, the scattering function for valence excitation can be written as

$$T^{(V)} \approx \left[\frac{e^2 \hbar V_s}{\pi\varepsilon_0}\right] \theta(\tau) \int_0^\infty d\omega \; Im\left(-\frac{1}{\varepsilon(\tau,\omega)}\right) \frac{1}{\tau^2+(\omega/v)^2} . \quad (28)$$

The result derived based on the mixed dynamic form factor is in agreement with Eq. (28) (Wang, 1992b).

Many-beam dynamical TDS calculations

TDS is used to demonstrate the application of Eq. (14) for inelastic electron diffraction pattern calculations. A multislice program for simulating high resolution electron microscopy images is modified to calculate the inelastic TDS electron diffraction patterns (Wang, 1992b). In the simulations for Mo (001) TDS diffraction patterns, a large unit cell was chosen with dimensions of 3.14 × 3.14 nm, divided by 256 × 256 pixels. The incident electron beam was assumed to be a plane wave (i.e., zero convergence). Thus the calculated diffraction patterns correspond to selected area diffraction (SAD) patterns in experiments. The phonon dispersion relationship derived under the central force approximation for monoatomic b.c.c. crystals was used in the calculation (Born 1942). A calculation for a crystal of thickness 188.4 nm took about 13 hrs on a DEC station 5000/200.

Figure 1 shows a comparison of a simulated Mo (001) elastic and TDS electron diffraction pattern with an experimentally observed SAD pattern. The experimental pattern shown in Fig. 1b is an energy-unfiltered diffraction pattern containing contributions from electrons that have experienced various elastic and inelastic scattering processes, such as plasmon excitations. The TDS streaks would be expected to appear sharper if the energy-filter is used (Reimer et al., 1990). The observed Kikuchi pattern is the result of valence, phonon and single electron excitations. This may be the reason that the crystal thickness assumed in theoretical calculations is considerably larger than the foil thickness used to take a corresponding diffraction pattern, because the scattering result of only one inelastic scattering process is used theoretically to fit the observed pattern of three inelastic processes. The simulated pattern is a sum of the contributions from purely elastically scattered electrons and phonon scattered electrons. The calculated pattern is displayed on a logarithmic scale in order to enhance the weak features of TDS streaks at large angles. The TDS streaks clearly appear along <010> and <100> corresponding to the observation in Fig. 1b. Thus, all the major features of these results are in good agreement. Similarly, good agreement has also been achieved for Si (001) (Fig. 2). The TDS streaks along <110> are clearly shown.

A 2-D lattice vibratiuon model

Dynamical calculations for electron diffraction are quite time consuming and complex. It is often helpful to have simplified models which can give qualitative results without any numerical calculations. In this section, we introduce a 2-D lattice vibration model for analyzing TDS streaks observed in electron diffraction patterns (Honjo et al., 1964). As pointed out above, the sharpness of TDS streaks is not affected by dynamical diffraction effects. Thus the streak directions and line shapes can be qualitatively predicted by examining the function

$$S_{TDS} \sim \sum_{j=1}^{3n_0} \int_{BZ} dq_z \frac{1}{\omega_j(\mathbf{q})} \frac{\exp(\hbar\omega_j(\mathbf{q})/k_BT)}{\exp(\hbar\omega_j(\mathbf{q})/k_BT) - 1} , \quad (29)$$

which is obtained from Eqs. (20) and (21) and is determined by the phonon dispersion relationship. The optical branches, for which ω varies slowly when **q** approaches zero, contribute a diffuse background in the diffraction pattern. The sharp streaks are produced by the acoustic branches, for which ω tends to zero when q approaches zero (Komatsu and Teramoto, 1966). For the high temperature limiting case, Eq. (29) becomes

$$S_{TDS}(\tau) \sim \frac{k_BT}{\hbar} \sum_{j=1}^{3n_0} \int_{BZ} dq_z \frac{1}{\omega_j^2(\tau,q_z)} . \quad (30)$$

In the phonon spectrum, there are $j = 3n_0$ branches of modes, of which only three are acoustic branches. The summation over j can be reduced to 3 if one is interested only in TDS streaks.

For a monoatomic crystal, under the central force approximation and from Eq. (8b), the phonon dispersion relation $\omega_j(\mathbf{q})$ is approximately related to atom positions by (Born, 1942),

$$\omega^2_j(\mathbf{q}_\perp=\tau, q_z) \sim \frac{F}{2m} \sum_{\ell\ell_1} \sum \sin^2[(\tau\cdot(\mathbf{r}(\ell)-\mathbf{r}(\ell_1)) + q_z z(\ell))/2]. \quad (31)$$

For atoms not confined to the same atomic (hkl) plane, i.e., $z(\ell) \neq 0$, $\omega^2_j(\mathbf{q})$ does not approach to zero for $\tau\bullet\mathbf{r}(\ell) = 0$ and $q_z \neq 0$. Therefore, the phonon modes with wave vectors **q** not confined to the diffraction plane (i.e., $q_z \neq 0$) may contribute only a diffuse background in the diffraction pattern. These modes do not have to be considered if one is interested only in TDS streaks.

In electron diffraction, if only the intensity distribution within the zero-order Laue zone (ZOLZ) is considered, the TDS is mainly generated by the phonon modes with wave vectors **q** parallel or almost parallel to the diffraction plane, because the momentum transferred from the incident electrons is almost restricted to this plane, and $q_z \approx K\,\hbar\omega/2E \approx 0$ for $\hbar\omega = 0.1$ eV and E = 100 keV. Bearing in mind the conservation of momentum and according to the discussions above, the sharp intensity variations can be considered to be generated by the atomic vibrations within the plane perpendicular to the incident beam direction, which is actually a 2-D lattice vibration model. Thus Eq. (30) can be approximated to

$$S_{TDS}(\tau) \sim \sum_{j=1}^{2} \frac{1}{\omega_j(\tau)} , \quad (32)$$

where $\omega_j(\tau)$ is defined as the dispersion surface of the acoustic branches determined by the 2-D atomic vibrations within the (hkl) plane when **B** = [hkl] (for orthogonal crystal systems). In following analyses, only the interactions between an atom and its neighbors, located in the same (hkl) atomic plane and closest to the atom are considered. In other words, the neighbors located closest to the atom but falling out of the 2-D plane will not be considered. This proposed 2-D vibration model will be applied in following analyses.

Monoatomic f.c.c. oriented in (001)

For f.c.c. metals oriented in (001), if only the interactions between an atom and its first nearest neighbors located at $\pm\frac{a}{2}[110]$ and $\pm\frac{a}{2}[1\bar{1}0]$ in the same (001) plane are considered, the phonon dispersion relationships are determined (Brüesch, 1982) by

$$\begin{bmatrix} D_{xx} & D_{xy} \\ D_{yx} & D_{yy} \end{bmatrix} \begin{bmatrix} e_{xj} \\ e_{yj} \end{bmatrix} = \omega_j^2 \begin{bmatrix} e_{xj} \\ e_{yj} \end{bmatrix}, \quad (33)$$

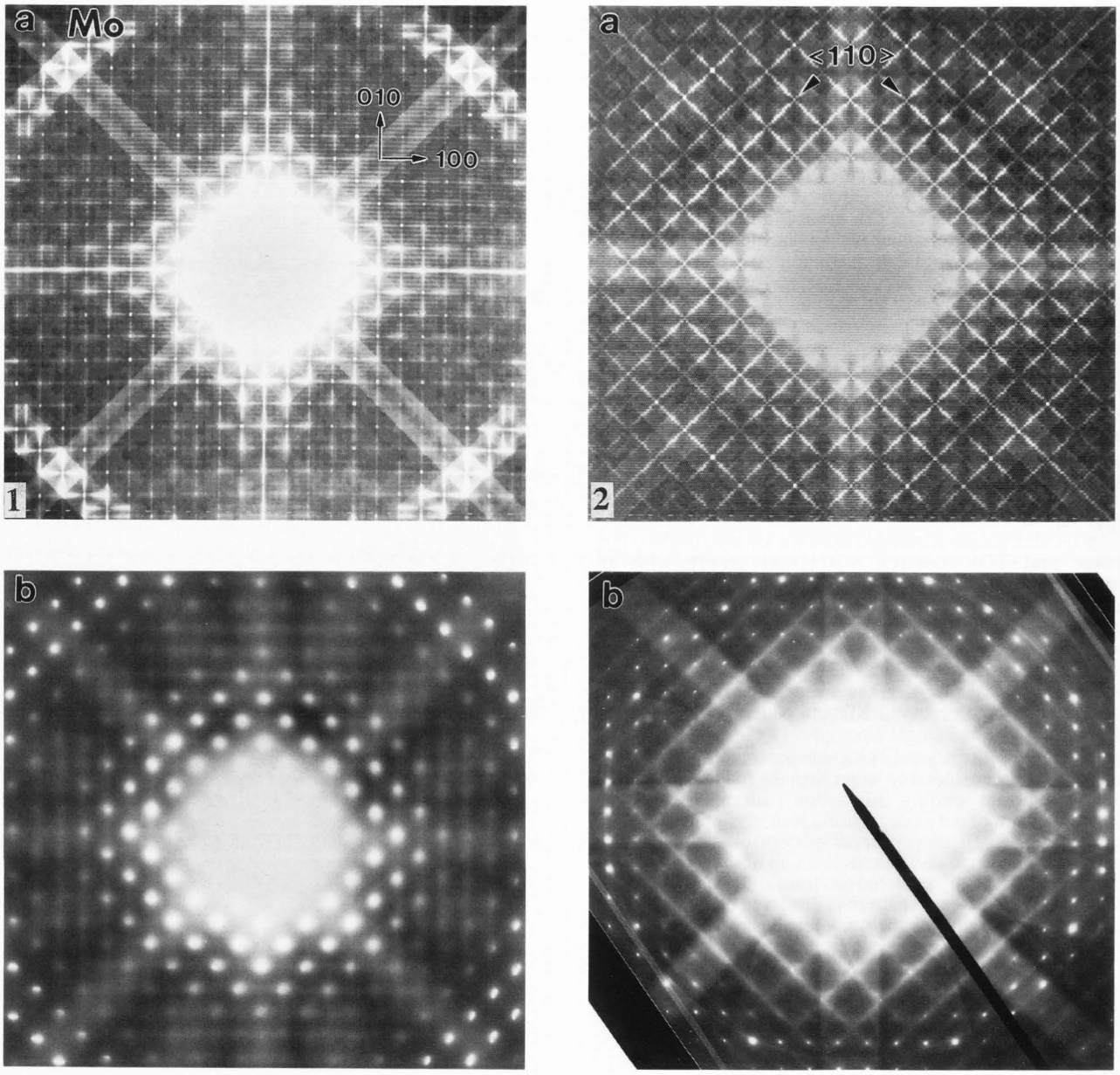

where

$$D_{xx} = D_{yy} = \frac{4F}{M}\left[\sin^2\frac{a}{4}(q_x+q_y) + \sin^2\frac{a}{4}(q_x-q_y)\right]; \quad (34a)$$

$$D_{xy} = D_{yx} = \frac{4G}{M}\left[\sin^2\frac{a}{4}(q_x+q_y) - \sin^2\frac{a}{4}(q_x-q_y)\right]. \quad (34b)$$

The non-trivial solution of Eq. (33) is determined by conditions

$$(\omega_{1,2})^2 = \frac{4}{M}\left[(F+G)\sin^2\frac{a}{4}(q_x \pm q_y) + (F-G)\sin^2\frac{a}{4}(q_x \mp q_y)\right]. \quad (35)$$

Fig. 1. Comparisons of (a) a simulated Mo (001) elastic and TDS electron diffraction pattern with (b) an observed SAD pattern. The crystal thickness is 1884 Å. Electron energy is 100 keV. The simulated diffraction pattern is the total contribution from elastic scattering and phonon scattering. The average momentum transfer was taken as $\mathbf{q}_1$ = <110>/6.28 Å^{-1}, where a is the lattice constant. The TDS streaks along <010> and <100> are clearly seen.

Fig. 2. Comparisons of (a) a simulated Si (001) elastic and TDS diffraction pattern with (b) an observed SAD pattern. The crystal thickness is 2443.5 Å. Electron energy is 100 keV, and $\mathbf{q}_1$ = <110>/a, where a = 5.43 Å. The TDS streaks along <110> are clearly seen.

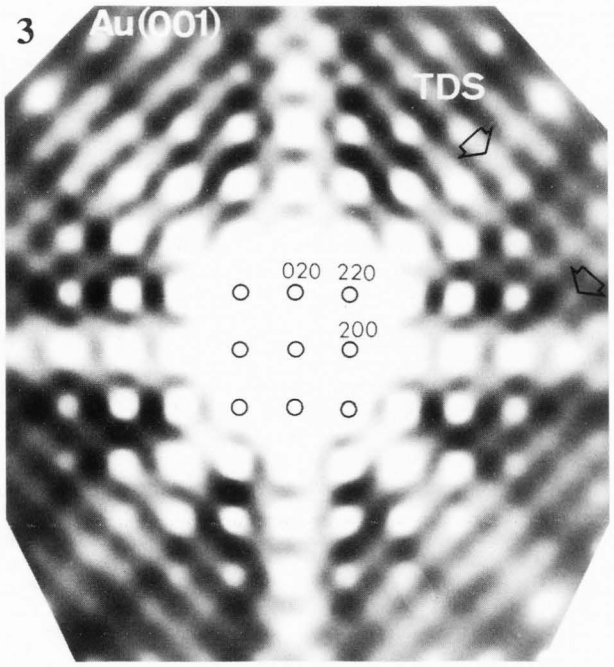

Fig. 3. TDS streaks observed in a SAD pattern of Au (001).

Changing **q** to τ, thus,

$$S_{TDS} \sim \frac{1}{[\sin^2 \frac{a}{4}(\tau_x \pm \tau_y) + \frac{F\text{-}G}{F+G} \sin^2 \frac{a}{4}(\tau_x \mp \tau_y)]^{1/2}}. \quad (36)$$

For simplicity, assume $F \approx G$, which is exact in the central force model (Born, 1942). For Au, $F = 1.937\times10^4$ dynes/cm and $G = 2.07\times10^4$ dynes/cm. It is expected that there are intensity walls located at $\tau_x \pm \tau_y = 0$ (i.e., <110>). This agrees to the observation for Au (Fig. 3). The sharpness of the walls determines the widths of TDS streaks in the diffraction pattern. In practice, it is usually the case that $F \neq G$ and $|F\text{-}G| << F$. Thus the $(F\text{-}G)/(F+G) \sin^2 \frac{a}{4}(q_x \pm q_y)$ terms determine the width of the TDS streaks. In other words, the width of the TDS streaks is determined by the non-central interaction force between atoms. The diffraction pattern shown in Fig. 3 was taken with a slightly convergent beam. The diameters of the diffraction spots are limited by the beam convergence, because it was difficult to find a large, unbent, thin, single crystal Au foil in practice.

Monoatomic b.c.c. oriented in (001)

As for f.c.c. metals, one can obtain dispersion relations for b.c.c. metals if only the interactions between the first nearest neighbors separated by a in the (001) plane are considered, i.e., the interactions of atoms 1 with 2, 2 with 3, 3 with 4, and 4 with 1 (see the model shown in Fig. 4a),

$$(\omega_{1,2})^2 = \frac{4}{M}[(F+G) \sin^2 \frac{a}{2} q_{x,y} + (F\text{-}G) \sin^2 \frac{a}{2} q_{y,x}]. \quad (37)$$

For F = G, one has,

$$S_{TDS} \sim \{\frac{1}{|(\sin \frac{a}{2}\tau_{x,y})|}\}, \quad (38)$$

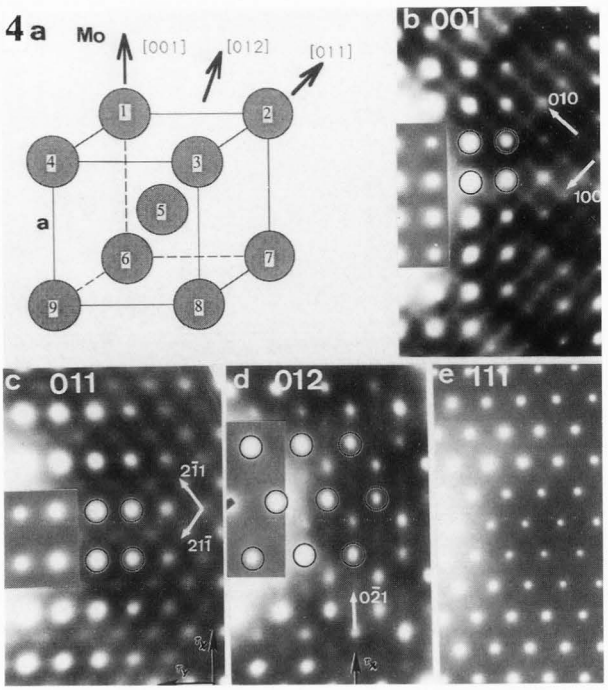

Fig. 4. a) An atomic model of b.c.c. monoatomic lattice; b) to e) are electron diffraction diffraction patterns taken from a Mo b.c.c. single crystal to show the TDS streaks observed when the beam direction is [001], [011], [012] and [111], respectively. τ_x and τ_y indicate the vectors used in theoretical investigations. The positions of the regular Bragg reflections due to pure elastic scattering are circled.

and it is expected that the sharp TDS streaks would be along <100> and <010>. For Mo, since $F = 3.61\times10^4$ dynes/cm and $G = 2.79\times10^4$ dynes/cm, $F \approx G$ is not a good approximation, so that the TDS streaks may be broadened by the (F-G) term contained in ω^2. This is in agreement with the experimental observations of Mo (001) shown in Fig. 4b.

Monoatomic b.c.c. oriented in (011)

For b.c.c. metals oriented in (011), if the interactions between atoms 5 and 1, 4, 7 and 8, separated by $\frac{a}{2}$<111> are considered (see the model in Fig. 4a),

$$(\omega_{1,2})^2 = \frac{4}{M}[(F+G) \sin^2 \frac{a}{4}(q_x \pm \sqrt{2}\, q_y) + (F\text{-}G) \sin^2 \frac{a}{4}(q_x \mp \sqrt{2}\, q_y)]. \quad (39)$$

It must be pointed out that $\tau = (\tau_x, \tau_y)$ is always defined in the plane perpendicular to the incidence beam direction, which should be distinguished from the indices of the diffraction pattern. Thus,

$$S_{TDS} \sim \{\frac{1}{|\sin \frac{a}{4}(\tau_x \pm \sqrt{2}\tau_y)|}\}, \quad (40)$$

and the TDS lines satisfy $\tau_x \pm \sqrt{2}\tau_y = 0$ in the diffraction plane. Converting τ to the indices of the diffraction pattern, it

is expected that the TDS streaks would be along $\pm[21\bar{1}]$ and $\pm[2\bar{1}1]$. A corresponding experimental observation of Mo (011) is shown in Fig. 4c. The intersections of the $\pm[21\bar{1}]$ and $\pm[2\bar{1}1]$ streaks show stronger intensity and appear like weak reflected "spots". These "spots" are at the positions of Bragg reflections in the first order Laue zone.

Monoatomic b.c.c. oriented in (012)

If one views the b.c.c. lattice along the [012] direction, the closest arranged atoms are atoms 1 and 4 (see Fig. 4a), thus

$$\omega^2 = \frac{4}{M} F \sin^2 \frac{a}{2} q_x, \tag{41}$$

and

$$S_{TDS} \sim \{ \frac{1}{|\sin \frac{a}{2}\tau_x|} \}, \tag{42}$$

and the TDS line satisfies $\tau_x = 0$ in the diffraction plane. After considering the correspondence of the diffraction spots with the atomic planes in the crystal unit cell, the streaks are expected along $\pm[0\bar{2}1]$, which is observed experimentally for Mo (012) (Fig. 4d). Besides the circled Bragg reflections, some weak streaks are also observed, which are the result of phonon scattering.

Monoatomic b.c.c. oriented in (111)

For b.c.c. metals oriented in (111), the closest atoms arranged in the (111) plane are separated by a<110>. This distance may be so large that the interactions between the atoms within the 2-D plane become weak. In this case, there may be no TDS streaks but only a diffuse background in the diffraction pattern. The corresponding observation of Mo is shown in Fig. 4e. This shows an important fact that atoms located further away than $\sqrt{2}a$ in Mo do not have strong interactions.

The interpretation of TDS line sharpness as being due to long-range atomic interactions may not be correct, because long-range interactions produce not only the basic streaks expected from the first nearest neighbor interactions, but also introduce equally intense TDS lines located between and parallel to the basic streaks. These "extra" lines have not been observed experimentally. Only the interactions with the first nearest neighbors are important in qualitative TDS interpretations. It is necessary to point out that nearest neighbor interaction can lead to long range phase correlation.

From the discussion above, it seems that a general relationship $S_{TDS}(\tau) \sim 1/\omega_j \sim 1/|\sin(\tau \bullet (\mathbf{r}(l)-\mathbf{r}(l_1))/2)|$ is approximately held for monoatomic cubic systems under the central force approximation. Thus S_{TDS} becomes infinite when $\tau \bullet (\mathbf{r}(l)-\mathbf{r}(l_1)) = 0$. Therefore, the directions of TDS streaks predicted according to the procedures above are consistent with those predicted according to the $\tau \bullet (\mathbf{r}(l)-\mathbf{r}(l_1)) = 0$ rule, which was proposed by Wang and Bentley (1991a) based on semi-classical theory. If the electron beam direction $\mathbf{B} = [hkl]$ and $\mathbf{r}(l)-\mathbf{r}(l_1) = (H_1\mathbf{a}_1, K_1\mathbf{a}_2, L_1\mathbf{a}_3)$, since $\tau \bullet \mathbf{B} = 0$ in the diffraction plane, the TDS streak produced by this nearest-neighbor interaction would be along $\tau = [\mathbf{r}(l)-\mathbf{r}(l_1)] \times \mathbf{B}$, i.e.,

$$\tau = \begin{vmatrix} \mathbf{a}_1^* & \mathbf{a}_2^* & \mathbf{a}_3^* \\ H_1 & K_1 & L_1 \\ h & k & l \end{vmatrix} \tag{43}$$

where $\mathbf{a}_1^*$ to $\mathbf{a}_3^*$ are the lattice vectors in reciprocal space. The readers can check the validity of this rule for the TDS streaks observed in Figs. 2-4.

Double-inelastic scattering processes

Phonon, single-electron and valence excitations coexist in electron diffraction. It is possible that an incident electron can undergo two or more different inelastic scattering processes when interacting with a crystal. This is the plural inelastic scattering process in electron diffraction. Consider now the cases of double-inelastic scattering. The crystal can be considered as either in its ground state (elastic) or in one of its two "independent" excited states. By independent one means that the excitation of each state is not affected by the other one and can be treated separately, such as single-electron and phonon excitations. The transitions from the ground state to each of the two states can be described by Eq. (4a). If the transition matrix elements are denoted by $U_{(1)} = U_{10}$ for $\phi_{(1)}$ and $U_{(2)} = U_{20}$ for $\phi_{(2)}$, the double scattering (ϕ_D) can only be either from process (or event) $\phi_{(1)}$ to process $\phi_{(2)}$ or from $\phi_{(2)}$ to $\phi_{(1)}$ (see Fig. 5a). This treatment has separated the double inelastic scattering into two single step processes; the direct scattering (or one-step process) of the electrons from the ground state (ϕ_0) to the final inelastic state (ϕ_D) (such as the excitation of a double plasmon, for an example) is neglected. This direct scattering is usually termed the "coherent" inelastic scattering (for double-plasmon excitations see Spence and Spargo, 1971) and is typically small in practice. Thus, according to Eqs. (4a) and (7a), one has (Wang, 1991)

$$\begin{aligned} \frac{\partial \phi_D(\mathbf{r})}{\partial z} &= \alpha\{U_{(2)}(\mathbf{r})\, \phi_{(1)}(\mathbf{r}) + U_{(1)}(\mathbf{r})\, \phi_{(2)}(\mathbf{r})\} \\ &= \alpha^2\{(U_{(2)}(\mathbf{r}) \int_0^z dz_1\, U_{(1)}(\mathbf{b},z_1) \\ &\quad + U_{(1)}(\mathbf{r}) \int_0^z dz_1\, U_{(2)}(\mathbf{b},z_1)\}. \end{aligned} \tag{44}$$

In Eq. (44), the electrons which undergo inelastic event 1 first then event 2 or event 2 first then event 1 would have the same shift; thus they can be treated as coherent. The first term in Eq. (44) means the inelastically scattered wave generated at depth z_1 by the event 1 is being inelastically scattered (event 2) again at depth z after being elastically scattered from z_1 to z. An equivalent interpretation applies to the second term. The solution of Eq. (44) is

$$\phi_D(\mathbf{r}) = \alpha^2 \left\{ \int_0^z dz_1\, U_{(1)}(\mathbf{b},z_1) \int_0^z dz_1'\, U_{(2)}(\mathbf{b},z_1') \right\}, \tag{45}$$

which satisfies the boundary condition $\phi_D(\mathbf{b},z=0) = 0$. Putting Eqs. (45) and (7b) into Eq. (2), the double-scattered wave at the exit face of the crystal z = d is

$$\begin{aligned} \Psi_D(\mathbf{b},d) = \alpha^2\{ &\int_0^d dz_1\, H'_{(1)}(\mathbf{b},z_1,\mathbf{q}) S_{(1)}(\mathbf{b},z_1) \\ &\times \int_0^d dz_1'\, H'_{(2)}(\mathbf{b},z_1',\mathbf{q}') S_{(2)}(\mathbf{b},z_1')) \Psi_D^0(\mathbf{b},d), \end{aligned} \tag{46a}$$

where

$$S_{(n)}(\mathbf{b},z) \equiv \Psi_0^0(\mathbf{b},z) / \frac{\partial \Psi_{(n)}^0(\mathbf{b},z)}{\partial z}, \tag{46b}$$

$\Psi_{(1)}^0$, $\Psi_{(2)}^0$ and Ψ_D^0 are the elastically scattered waves of incident electrons of wave vectors $\mathbf{k}_{(1)}$, $\mathbf{k}_{(2)}$ and $\mathbf{k}_D$, respectively; and $H'_{(1)}$ and $H'_{(2)}$ are the interaction

Hamiltonians for process 1 (of momentum transfer $\mathbf{q}$) and 2 (of momentum transfer $\mathbf{q}'$), respectively. The physical meaning of Eq. (46a) can be simply stated as follows. The double inelastic waves can be generated at any point inside the specimen with a probability function proportional to $|H'_{(1)}H'_{(2)}|^2$. The inelastic events occurring at different atom locations are marked with a "historical tag", $S_{(n)} = \Psi^0_0(\mathbf{r})/\frac{\partial \Psi^0_{(n)}(\mathbf{r})}{\partial z}$, which is responsible for the formation of Kikuchi lines; the elastic scattering of those electrons after a single inelastic excitation is the same as the elastic scattering of incident electrons with equivalent energy and momentum. The calculation of $S_{(n)}$ in the multislice scheme is given in Appendix B. Following procedures analogous to those used for deriving Eq. (14), taking a 2-D Fourier transform of Eq. (46a), yields

$$\Psi_D(\tau,d) = \left(\frac{4\pi^2\alpha}{A}\right)^2 \sum_{\mathbf{g}}\sum_{\mathbf{g}'} H'^{(1)}_{\mathbf{g}}(\mathbf{g}-\mathbf{q})\, H'^{(2)}_{\mathbf{g}'}(\mathbf{g}'-\mathbf{q}') \times Z_2(\tau-\mathbf{g}+\mathbf{q}_b-\mathbf{g}'+\mathbf{q}_b',\mathbf{q},\mathbf{q}'), \quad (47)$$

where

$$Z_2(\tau,\mathbf{q},\mathbf{q}') \equiv \left[\int_0^d dz\ \exp(iq_z z)\, S_{(1)}(\tau,z)\right] \otimes \left[\int_0^d dz'\ [\exp(iq_z' z')\, S_{(2)}(\tau,z')\right] \otimes \Psi^0_D(\tau,d); \quad (48)$$

Summing the intensities contributed by the inelastic scattering processes of different $\mathbf{q}$ and $\mathbf{q}'$ incoherently, and after some calculation, one finally obtains

$$I_D(\tau) = \left(\frac{V_c}{(2\pi)^3}\right)^2 \int_{BZ} d\mathbf{q} \int_{BZ} d\mathbf{q}'\ |\Psi_D(\tau,d)|^2 \approx \xi^4 \left\{T^{(2)}(\tau) \otimes T^{(1)}(\tau) \otimes |Z_2(\tau,\mathbf{q}_1,\mathbf{q}_2)|^2\right\}, \quad (49)$$

where $\mathbf{q}_1$ and $\mathbf{q}_2$ are the average momentum transfers involved in inelastic processes 1 and 2, respectively. Therefore, the diffraction patterns for valence-phonon, valence-single electron and valence-valence double excitations can be obtained with the use of corresponding $T^{(V)}$ (Eq. (28)), $T^{(TDS)}$ (Eq. (21)) and $T^{(S)}$ (Eq. (27)) in Eq. (49). The lengthy results will not be listed here.

Multiple inelastic scattering theory

Before proposing the multiple scattering theory, one considers a triple scattering process (ϕ_T). The crystal can be considered as either in its ground state (elastic) or in one of its three "independent" excited states. The transitions from the ground state to each of the three states can be described separately by Eq. (7a) . An electron can be scattered in 3! different sequences among the three inelastic states (see Fig. 5b). Using the double scattering result in Eq. (45) and through Eq. (4a), one obtains for triple inelastic scattering

$$\frac{\partial \phi_T(\mathbf{r})}{\partial z} = \alpha^3\{U_{(3)}(\mathbf{r}) \int_0^z dz_2\, U_{(2)}(\mathbf{b},z_2) \int_0^z dz_1\, U_{(1)}(\mathbf{b},z_1) + U_{(2)}(\mathbf{r}) \int_0^z dz_2\, U_{(1)}(\mathbf{b},z_2) \int_0^z dz_1\, U_{(3)}(\mathbf{b},z_1) + U_{(1)}(\mathbf{r}) \int_0^z dz_2\, U_{(2)}(\mathbf{b},z_2) \int_0^z dz_1\, U_{(3)}(\mathbf{b},z_1)\}. \quad (50)$$

5a) Double inelastic scattering:

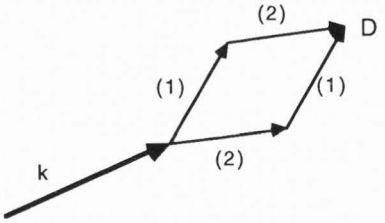

b) Triple inelastic scattering:

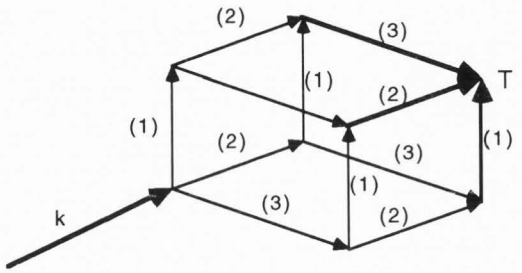

Fig. 5. Schematic models showing a) double- and b) triple-"independent" inelastic scattering processes in high energy electron diffraction, where (n), n = 1, 2 ... means the n^{th} inelastic scattering process or event.

The solution of Eq. (50) is

$$\phi_T(\mathbf{r}) = \alpha^3\{(\int_0^z dz_3\, U_{(3)}(\mathbf{b},z_3) \int_0^z dz_2\, U_{(2)}(\mathbf{b},z_2) \times \int_0^z dz_1\, U_{(1)}(\mathbf{b},z_1)\}. \quad (51)$$

It can be generalized from Eqs. (45) and (51) that the electron wave function after being multiply inelastically scattered m times among the m states is (Wang, 1991)

$$\phi_m(\mathbf{r}) = c_0\, \alpha^m \prod_{n=1}^{m} \int_0^z dz_n\, U_{(n)}(\mathbf{b},z_n) \quad \text{for } m \geq 1; \quad (52a)$$

$$\phi_0(\mathbf{r}) = c_0; \quad (52b)$$

A constant c_0 is introduced in Eq. (52) to take into account the absorption effect in order to normalize the total scattering intensity. Following procedures analogous to those used from Eq. (45) to Eq. (49), the intensity distribution contributed by the m^{th} multiple inelastic scattering in reciprocal space is

$$I_m(\tau) = (c_0\, \xi^m)^2 \left\{T^{(m)}(\tau) \otimes T^{(m-1)}(\tau) \otimes \cdots \otimes T^{(1)}(\tau)\right\} \otimes |Z_m(\tau,\mathbf{q}_1,\mathbf{q}_2,\ldots,\mathbf{q}_m)|^2, \quad (53a)$$

where

$$Z_m(\tau,\mathbf{q}_1,\mathbf{q}_2,\ldots,\mathbf{q}_m) \equiv F_{(m)}(\tau,\mathbf{q}_m) \otimes F_{(m-1)}(\tau,\mathbf{q}_{m-1}) \otimes \cdots \otimes F_{(1)}(\tau,\mathbf{q}_1) \otimes \Psi^0_0(\tau,d), \quad (53b)$$

$$F_{(m)}(\tau,\mathbf{q}_m) = \int_0^d dz\ \exp(iq_{(m)}z)\, S_{(m)}(\tau,z), \quad (54a)$$

and $$q_{(m)} = k_m \frac{E-E_m}{2E} . \quad (54b)$$

The physical meaning of Eq. (53a) can be understood as follows. The effects of multiple scattering are equivalent partially to broadening the single scattering function ($T^{(n)}$) by those of other processes, and partially to re-scattering the Kikuchi patterns ($|F_{(1)} \otimes \Psi_0^0|^2$) produced in one single scattering process by others. The convolution operations of $F_{(n)}$ functions in Eq. (53b) mean the convolutions of Kikuchi patterns produced by different inelastic scattering processes.

Valence excitations in HREM image simulations

In high-energy electron diffraction and imaging, valence excitations are delocalized inelastic scattering processes of many excited states of different energies and momentum transfers. The incoherence of the electrons in these excited states makes the theoretical treatment extremely difficult because the electrons that have excited a specific state have to be considered as a single stream propagating through the rest of the crystal. The diffraction pattern is formed by the incoherent sum of these different streams at the exit face of the crystal. Now this problem can be easily solved using Eq. (7a).

In high resolution electron microscopy (HREM), valence excitations contribute significant details to the images and become more important if the crystal is thicker (Stobbs and Saxton, 1988; Tang et al., 1989; Krivanek et al., 1990). Theoretical calculations of these authors are based on a model in which the valence excitation is considered as occurring at the entrance face of the crystal slab, the final image being an incoherent superposition of all the electrons with different incident energies. This model was introduced by assuming that the valence excitation is a perfectly delocalized inelastic scattering process, so that whether the inelastic events occur inside or outside the crystal does not affect the image calculations. This model, in principle, is valid for very thin crystals. However, two important questions remain: how thin should the crystal be to ensure the validity of the model and can we introduce a general theory for relatively thick crystals? In order to address these questions, we can start at Eq. (7a). Incoherently summing the intensities contributed by different valence states at the crystal exit face, and through some algebra (see Wang and Bentley, 1991b and c for details), the HREM image formed by valence-loss electrons of different energy losses $\hbar\omega$ is

$$I_v(\mathbf{b}) \approx k_0^2 \int_0^\infty d\omega \frac{dI_{EELS}(\omega)}{d\hbar\omega} | Y(\mathbf{b},E_0-\hbar\omega) \otimes F_{OB}(\mathbf{b},\omega) |^2, \quad (55)$$

where $\otimes$ indicates the convolution of $\mathbf{b}$; F_{OB} represents the effect of the objective lens on electrons of energy $E_0-\hbar\omega$, the Fourier transform of which is defined in reciprocal space as

$$F_{OB}(\tau,\omega) = B(\tau) \exp(iW(\tau)), \quad (56a)$$

with $$W(\tau)= \lambda(\omega)\tau^2[C_s\lambda(\omega)^2\tau^2/8\pi^2 - \Delta f(\omega)]/4\pi^2; \quad (56b)$$

the electron energy loss function is defined as

$$\frac{dI_{EELS}(\omega)}{d\hbar\omega} = \frac{\pi e^2 m_e^2}{\pi\varepsilon_0\hbar^3 k_0^2} \ln[\tau_c^2+(\frac{k_0\hbar\omega}{2\gamma E_0})^2] \, Im[- \frac{1}{\varepsilon(\omega)}]; \quad (57a)$$

and $Y(\mathbf{b},E)$ is the Fourier transform of the Y function defined by

$$Y(\mathbf{b},E) = \Psi_0^0(\mathbf{b},d,E) \int_0^d dz \, \Psi_0^0(\mathbf{b},z,E_0) / \frac{\partial\Psi_0^0(\mathbf{b},z,E)}{\partial z} , \quad (57b)$$

where $\Psi_0^0(\mathbf{b},z,E_0)$ and $\Psi_0^0(\mathbf{b},d,E)$ are the multislice solutions of Eq. (3) for electron incident energies E_0 and $E = E_0 - \hbar\omega$, respectively. The $Y(\mathbf{b},E)$ function partly characterizes the localization effect of valence excitations and partly represents the diffraction of the incident waves of different energies by the crystal. The inelastic wave of a particular state excited at crystal depth z is denoted by a location "tag", $S_{10} = \Psi_0^0(\mathbf{b},z,E_0) / \frac{\partial\Psi_0^0(\mathbf{b},z,E_0-\hbar\omega)}{\partial z}$. This function is responsible for the elastic re-scattering of the electrons after inelastic excitation and is the source of Kikuchi patterns. This localization effect is contained in S_{10}. For very small energy losses, i.e., $\omega \rightarrow 0$, $S_{10} \approx 1/ik_z$. Thus the localization effect becomes unimportant. For energy-losses larger than a few eV, the $\mathbf{b}$ variation of the S_{10} function becomes more and more significant with increasing of the crystal thickness d. In this case, the localization effect becomes important. All these effects are comprehensively included in Eq. (55).

As stated by Eq. (55), a full dynamical calculation is required for each different energy-loss. For small energy-losses, it has been found that the primary effect of valence-loss is to introduce a spherical aberration effect. Therefore, $Y(\mathbf{b},E_0-\hbar\omega) \approx Y(\mathbf{b},E_0)$. For relatively large energy-losses, it is possible to calculate $Y(\mathbf{b},E_0-\hbar\omega)$ based on the perturbation theory (Wang and Bentley, 1991b).

It is important to point out that Eq. (55) was derived based on the single inelastic scattering model. In practice, plural plasmon excitation obeys the Poission distribution, hence the relative intensity of the m^{th} plasmon loss to the pure elastic peak is $\frac{(d/\Lambda)^m}{m!}$, where Λ is the plasmon mean free path length and is typically about 100 - 200 nm for 400 keV electrons (Raether, 1980). For 400 keV, in the crystal thickness range of about 50 nm, the condition $(d/\Lambda)^2 << 1$ is always satisfied. Therefore, in the thickness range for HREM imaging, the plural plasmon excitation can be neglected. In other words, the single plasmon scattering model is a good approximation. Therefore, Eq. (55) is applicable for simulating images of valence-loss electrons in crystal thicknesses generally used for HREM.

To see the physical meaning of Eq. (55) clearly, consider a case in which the crystal thickness is assumed to be very small. For delocalized valence excitations with energy-loss less than about 30 eV and angular spreading less than 0.1 mrad, their perturbation to the wave function of the high-energy electrons (typically 400 kV) may be neglected if the specimen is thin. One approximately has

$$S_{10}(\mathbf{r}) \approx \frac{\exp(-iq_n z)}{ik_0}, \quad (58)$$

where $q_n = \frac{k_0\hbar\omega}{2E_0}$, so that

$$Y(\mathbf{b},E) = \frac{\exp(-iq_n d) - 1}{k_0 q_n} \Psi_0^0(\mathbf{b},d,E). \quad (59)$$

For $q_n d << 1$, $Y(\mathbf{b},\omega) = \frac{d}{ik_0} \Psi_0^0(\mathbf{b},d,\omega)$, and Eq. (55) becomes

$$I_v(\mathbf{b}) \approx d^2 \int_0^\infty d\omega \frac{dI_{EELS}(\omega)}{d\hbar\omega} I_{els}(\mathbf{b},E_0-\hbar\omega), \qquad (60a)$$

where the image formed by the elastic electrons of incident energy E is

$$I_{els}(\mathbf{b},E) = | \Psi_0^0(\mathbf{b},d,E) \otimes F_{OB}(\mathbf{b},E) |^2. \qquad (60b)$$

Therefore, the inelastic image is formed by the incoherent addition of the electrons with different incident energies E, weighted by the intensity distribution in the EELS spectrum from the imaged area of the specimen. Physically, Eq. (60a) indicates that the non-localized valence excitations can be considered as occurring at the entrance face of the crystal for thin specimens. The final image contrast of the electrons after valence excitation is determined by the inelastic incident wave after penetrating the crystal, i.e. $\Psi_0^0(\mathbf{b},z,E)$ at the exit face z = d. It is not necessary to consider the detailed excitation processes of the valence electrons. This is the result of perfectly delocalized inelastic scattering.

Under the small thickness approximation, $q_n d<<1$, Eq. (60) establishes the wave mechanics basis of the model used by several authors (Stobbs and Saxton, 1988; Tang et al., 1989; Krivanek et al., 1990). The condition $q_n d=\frac{k_0 \hbar\omega d}{2\gamma E_0}<<1$ sets a criterion for identifying the applicability of the simplified theory (Eq. (60a)). For an energy loss of 20 eV and E_0 = 400 keV, this criterion yields d << 20 nm. Thus this simplified model can be considered as a reasonable treatment if the specimen thickness is about 5 nm or less. It is only in this thickness range that the valence excitation could be assumed to occur at the entrance face of the crystal, otherwise the localization effects of the valence excitation need to be considered. However, if the crystal is thinner than 5 nm, the contribution to the image by plasmon-loss electrons should be negligible compared to that made by the elastic electrons. For thicker crystals commonly used for HREM imaging, the contributions of valence-loss electrons may be significant, but the simplified model is inapplicable and calculations based on Eq. (55) would be necessary.

Summary and conclusions

A dynamical theory is proposed with which to calculate diffraction patterns formed by inelastically scattered electrons. The most important advantage of this new theory is that the incoherence of all the possible inelastic scattering processes of different energies and momenta can be evaluated analytically before any numerical calculations. A full quantum mechanical description is given for phonon or thermal diffuse scattering in electron diffraction. The TDS pattern is generated by a "convolution" of the lattice dynamics with the electron scattering dynamics. The former defines the shapes of TDS streaks and the latter determines the final intensity distribution in the diffraction pattern. It has been shown that the sharpness of TDS streaks appearing in the electron diffraction pattern is determined by the phonon dispersion relationships of acoustic branches, for which ω tends to zero when q approaches zero; optical branches contribute only a diffuse background.

A simplified 2-D atomic vibration model is introduced to predict the TDS streaks in electron diffraction patterns. The phonon modes corresponding to the interactions of nearest neighbors located out of the (hkl) atomic plane perpendicular to the incident beam may not contribute strongly in near zone axis cases. These modes also contribute only to the diffuse background in the diffraction pattern. It is only the interactions between the atoms with their first nearest neighbors located in the same 2-D (hkl) plane perpendicular to the beam **B** = [hkl] that are responsible for the orientation dependence of the sharp TDS streaks. Qualitative interpretations can be obtained by examining the $1/\omega_j(\mathbf{q})$ function, where $\omega(\mathbf{q})$ is the phonon dispersion relationships determined by the 2-D atomic vibrations in the (hkl) plane under the harmonic oscillator approximation. The TDS streaks are defined by the τ_x - τ_y curves satisfying $\omega_j(\tau) = 0$. It is shown that the width of the TDS streaks is dominated by the non-central interaction forces between atoms; the TDS streaks should appear perfectly sharp if the central force model holds exactly. The directions of TDS streaks predicted according to this theory are consistent with those predicted according to the $\tau\bullet(\mathbf{r}(\ell)-\mathbf{r}(\ell_1)) = 0$ rule, where the selection of ℓ_1 is restricted to the first nearest neighbors of the ℓ^{th} atom that are located in the same atomic plane as the ℓ^{th} atom perpendicular to the incident beam direction.

A dynamical multiple-elastic and -inelastic electron scattering theory is proposed for "independent" inelastic scattering events, where the excitation of each state is not affected by the other states and each can be treated separately using single-inelastic scattering theory. The plural scattering of phonon, single-electron and valence (or plasmon) excitations can be comprehensively included in a single formula. The scattering functions for these different types of inelastic scattering events have been derived. In this new theory, only the modulus square of the scattering matrix element is needed; the phase shift of inelastic scattering has been evaluated before any numerical calculation. In addition, the equivalence of this theory with the inelastic multislice theory has been proved.

A new theory is proposed with which to include the effects of valence excitations in image simulations for high-resolution electron microscopy (HREM), based on a single inelastic scattering model. Under the small thickness approximation (thinner than about 5 nm for 400 keV electrons), this general theory reduces to the simplified theory proposed previously by several others, in which the image can be considered as an incoherent sum of those produced by incident electrons of different energies weighted by the intensity distribution in the electron energy-loss spectrum, with due consideration for the objective lens chromatic aberration effects on electrons with different energy-losses. It is concluded that this simplified model has little use in practice because plasmon excitation should not be important if the crystal thickness is less than 5 nm. In a more general case, our new theory provides a feasible method for calculating the HREM images of valence excited electrons for thicker crystals.

Acknowledgement

We are grateful to Drs. D Van Dyck and K. Ishizuka for comments. This research was sponsored by the Division of Materials Sciences, U.S. Department of Energy, under contract DE-AC05-84OR21400 with Martin Marietta Energy Systems, Inc.

Appendix A: Equivalence of Eq. (7a) with the inelastic multislice theory

For easy notation, one separates the wave function from its plane wave part by defining

$$\Psi_n(\mathbf{r}) = \varphi_n(\mathbf{b},z) \exp(i\mathbf{k}_n\bullet\mathbf{r}), \qquad (A.1a)$$

$$\Psi_n^0(\mathbf{r}) = \varphi_n^0(\mathbf{b},z) \exp(i\mathbf{k}_n\bullet\mathbf{r}). \qquad (A.1b)$$

For the n^{th} excited state, Eq. (7a) can be rewritten as

$$\varphi_n(\mathbf{b},z) = \alpha \int_0^z dz' \left\{ H'_{n0}(\mathbf{b},z')\, \Psi_0^0(\mathbf{b},z') / \frac{\partial \Psi_n^0(\mathbf{b},z')}{\partial z} \right\} \varphi_n^0(\mathbf{b},z). \tag{A.2}$$

By neglecting the back scattering term under the small angle approximation, in the multislice method, the solution of the elastic Schrödinger equation can be written (Cowley and Moodie, 1957; Ishizuka and Uyeda, 1977) as

$$\varphi_n^0(\mathbf{b},z+\Delta z) = \left(\varphi_n^0(\mathbf{b},z)\, Q(\mathbf{b},z)\right) \otimes P_n(\mathbf{b}), \tag{A.3}$$

where Q is the phase grating function of the crystal slice Δz

$$Q(\mathbf{b},z) = \exp\left[i\sigma \int_z^{z+\Delta z} dz'\, V(\mathbf{b},z') \right]; \tag{A.4}$$

the wave propagation function is

$$P_n(\mathbf{b}) = \frac{1}{i\Delta z \lambda_n} \exp\left[\frac{i\pi b^2}{2\lambda_n \Delta z} \right]; \tag{A.5}$$

$\sigma = \dfrac{e}{\hbar v_0}$; v_0 is the electron velocity; and λ_n is the electron wavelength by energy E_n.

Now one derives the relationship which governs the inelastic wave $\varphi_n(\mathbf{b},z)$ before and after being scattered by a very thin crystal slice of thickness Δz. From Eq. (A.2), one can directly write

$$\begin{aligned}
&\varphi_n(\mathbf{b},z+\Delta z) - \varphi_n(\mathbf{b},z) \\
&= \alpha \int_0^z dz' \left\{ H'_{n0}(\mathbf{b},z')\, \Psi_0^0(\mathbf{b},z') / \frac{\partial \Psi_n^0(\mathbf{b},z')}{\partial z} \right\} \\
&\quad \times \left[\varphi_n^0(\mathbf{b},z+\Delta z) - \varphi_n^0(\mathbf{b},z) \right] \\
&\quad + \alpha \int_z^{z+\Delta z} dz' \left\{ H'_{n0}(\mathbf{b},z')\, \Psi_0^0(\mathbf{b},z') / \frac{\partial \Psi_n^0(\mathbf{b},z')}{\partial z} \right\} \\
&\quad \times \varphi_n^0(\mathbf{b},z+\Delta z) \\
&\approx \varphi_n(\mathbf{b},z) \left[\frac{\varphi_n^0(\mathbf{b},z+\Delta z)}{\varphi_n^0(\mathbf{b},z)} - 1 \right] \\
&\quad + \alpha \left\{ h'_{n0}(\mathbf{b},z)\, \Psi_0^0(\mathbf{b},z) / \frac{\partial \Psi_n^0(\mathbf{b},z)}{\partial z} \right\} \varphi_n^0(\mathbf{b},z+\Delta z),
\end{aligned} \tag{A.6}$$

$$\text{where} \quad h'_{n0} = \int_{z_0}^{z} H'_{n0}(\mathbf{b},z')dz'. \tag{A.7}$$

Equation (A.6) can be conveniently written as

$$\begin{aligned}
\varphi_n(\mathbf{b},z+\Delta z) &\approx \varphi_n(\mathbf{b},z) \left(\frac{\varphi_n^0(\mathbf{b},z+\Delta z)}{\varphi_n^0(\mathbf{b},z)} \right) \\
&\quad + \alpha \left\{ h'_{n0}(\mathbf{b},z) \Psi_0^0(\mathbf{b},z) / \frac{\partial \Psi_n^0(\mathbf{b},z)}{\partial z} \right\} \varphi_n^0(\mathbf{b},z+\Delta z).
\end{aligned} \tag{A.8}$$

For fast electrons, it is always a good approximation to assume forward scattering (see Appendix B), so that

$$\begin{aligned}
\frac{\partial \Psi_n^0(\mathbf{b},z)}{\partial z} &= \left[ik_{nz} \varphi_n^0(\mathbf{b},z) + \frac{\partial \varphi_n^0(\mathbf{b},z)}{\partial z} \right] \exp(i\mathbf{k}_n \bullet \mathbf{r}) \\
&\approx ik_{nz} \varphi_n^0(\mathbf{b},z) \exp(i\mathbf{k}_0 \bullet \mathbf{r}),
\end{aligned} \tag{A.9}$$

where an approximation of $\mathbf{k}_n \approx \mathbf{k}_0$ is made for thin specimens. Using Eq. (A.9), Eq. (A.8) becomes

$$\varphi_n(\mathbf{b},z+\Delta z) \approx \left[\varphi_n(\mathbf{b},z) - i\sigma h'_{n0}(\mathbf{b},z) \varphi_0^0(\mathbf{b},z) \right] \left(\frac{\varphi_n^0(\mathbf{b},z+\Delta z)}{\varphi_n^0(\mathbf{b},z)} \right). \tag{A.10}$$

The physical meaning of Eq. (A.10) can be interpreted as follows. The first term in [...] ($\varphi_n(\mathbf{b},z)$) is the inelastic wave generated before the wave arrives at the slice entrance face located at z = z. In the single inelastic scattering model, this part of the wave will be only elastically scattered when it penetrates the crystal slice and is thus responsible for the formation of Kikuchi patterns. The second term in [...] ($\sigma h'_{n0}\varphi_0$) is the newly inelastic wave generated when the elastic wave (φ_0^0) penetrates through the slice. The elastic scattering of these two parts within the slice is included in the term $\varphi_n^0(\mathbf{b},z+\Delta z)/\varphi_n^0(\mathbf{b},z)$. For very thin slices ($\Delta z \to 0$), P_n is very close to a Dirac δ function; using Eq. (A.3), Eq. (A.10) can thus be approximately written as

$$\begin{aligned}
\varphi_n(\mathbf{b},z+\Delta z) &= \left[\varphi_n(\mathbf{b},z) - i\sigma h'_{n0}(\mathbf{b},z) \varphi_0^0(\mathbf{b},z) \right] \\
&\quad \times \frac{\left(\varphi_n^0(\mathbf{b},z)\, Q(\mathbf{b},z)\right) \otimes P_n}{\varphi_n^0(\mathbf{b},z)} \\
&\approx \left[Q(\mathbf{b},z) \left\{ \varphi_n(\mathbf{b},z) - i\sigma h'_{n0}(\mathbf{b},z) \varphi_0^0(\mathbf{b},z') \right\} \right] \otimes P_n(\mathbf{b}).
\end{aligned} \tag{A.11}$$

Equation (A.11) is the exact form of the multislice theory for single inelastic scattering (Wang, 1989). This establishes the equivalence of Eq. (7a) with the other inelastic scattering theories.

Appendix B: Calculation of $S_{(n)}$ function in multislice scheme

For convenient notation, dropping the subscript n in Eq. (5b) and taking $U = H'_{nn}(\mathbf{r})$, Eq. (5b) can be written as

$$(\nabla^2 + k^2)\Psi^0 = \frac{2m_e}{\hbar^2} U(\mathbf{r})\Psi^0. \tag{B.1}$$

This equation is the standard elastic scattering equation of high energy electrons. By writing

$$\Psi^0 \equiv \varphi^0 \exp(i\mathbf{k} \bullet \mathbf{r}), \tag{B.2}$$

the calculation of φ^0 is governed by Eq. (A.3). In the multislice approach, a crystal is cut into many slices in the z direction and the atomic structure in each slice is projected onto a plane perpendicular to the z axis. It is not straightforward to find $\dfrac{\partial \Psi_n{}^0(\mathbf{r})}{\partial z}$ directly from $\Psi_n{}^0$ in the multislice approach.

For this reason one starts from Eq. (B.1). Putting Eq. (B.2a) into (B.1) and neglecting the $\frac{\partial^2\varphi^0}{\partial z^2}$ term, Eq. (B.1) becomes

$$\frac{\partial\varphi^0(\mathbf{r})}{\partial z} = \{\frac{2m_e}{\hbar^2}U(\mathbf{r})\varphi^0 - (\frac{\partial^2}{\partial x^2}+\frac{\partial^2}{\partial y^2})\varphi^0 - i2(k_x\frac{\partial}{\partial x}+k_y\frac{\partial}{\partial y})\varphi^0\}/i2k_z. \quad (B.3)$$

Reintroducing the n and m notation,

$$S_{(m)}(\mathbf{r}) = \frac{\varphi_0^0\exp(i(\mathbf{k}_0-\mathbf{k}_m)\bullet\mathbf{r})}{ik_{mz}\varphi_m^0+\frac{\partial\varphi_m^0(\mathbf{r})}{\partial z}} = \varphi_0^0\exp(i(\mathbf{k}_0-\mathbf{k}_m)\bullet\mathbf{r}) \times\{(ik_{mz}\varphi_m^0+[-\frac{2m_ee}{\hbar^2}V(\mathbf{r})\varphi_m^0-(\frac{\partial^2}{\partial x^2}+\frac{\partial^2}{\partial y^2})\varphi_m^0 - i2(k_{mx}\frac{\partial}{\partial x}+k_{my}\frac{\partial}{\partial y})\varphi_m^0]/i2k_{mz})\}^{-1}, \quad (B.4)$$

where the calculation of φ_0^0 and φ_m^0 is governed by Eq. (A.3). The momentum transfer during the inelastic transition from the m^{th} state to the n^{th} state is $\mathbf{q}_{mn} = \mathbf{k}_n - \mathbf{k}_m$. In Eq. (B.4), crystal potential V and the Laplace operator characterize the elastic re-scattering of the inelastic wave. Therefore, $S_{(m)}$ function is responsible for the formation of Kikuchi lines. For high energy electrons, to a good approximation, the first term in the denominator of (B.4) is much larger than the remaining terms; thus

$$S_{(m)}(\mathbf{r}) \approx \frac{\varphi_0^0\exp(i\mathbf{q}_{m0}\bullet\mathbf{r})}{ik_{mz}\varphi_m^0}. \quad (B.5)$$

References

Bird DM, Wright AG. (1989). Phase dependence of Kikuchi patterns. I. Theory. Acta Cryst. A**45**, 104-109.

Björkman G, Lundqvist BI, Sjölander A. (1967). Dampling of phonons in aluminum. Phys. Rev. **159**, 551-553.

Born M. (1942). Theoretical investigations on the relation between crystal dynamics and X-ray scattering. Rep. Prog. Phys. **9**, 294-333.

Brüesch P. (1982). Phonons: Theory and experiments I - Lattice dynamics and models of interatomic forces, Springer-Verlag Berlin Heidelberg New York 17-99.

Cowley JM, Moodie AF. (1957). The scattering of electrons by atoms and crystals I. A new theoretical approach. Acta. Cryst. A**10,** 609-619.

Cowley JM, Pogany AP. (1968). Diffuse scattering in electron diffraction patterns. I. General theory and computation method. Acta Cryst. A**24**, 109-116.

Doyle PA. (1971). Dynamical calculation of electron scattering by plasmons in aluminium. Acta Cryst. A**27**, 109-116.

Egerton RF. (1986). Electron energy-loss spectroscopy in electron microscope (Plenum Press, New York) 129-180.

Fanidis C, Van Dyck D, Van Landuyt J. (1990). Dynamical electron diffraction in a crystal with atoms in thermal motion. Proc. of XIIth Intern. Cong. for Electron Microscopy (Seattle), San Francisco Press, Vol. 1, eds. L. D. Peachey and D. B. Williams, 58-59.

Fanidis C, Van Dyck D, Coene W, Van Landuyt J. (1989). Thermal atom motion in the simulation of high resolution images and electron diffraction patterns. "Computer Simulation of Electron Microscope Diffraction and Images", Edited by W. Krakow and M. O'Keefe, The Minerals, Metals nd Materials Soc., 135-157.

Gjønnes J. (1966). The influence of Bragg scattering on inelastic and other forms of diffuse scattering of electrons. Acta Cryst. **20**, 240-249.

Gjønnes J, Watanabe D. (1966). Dynamical diffuse scattering from magnesium oxide single crystals. Acta Cryst. **21**, 297-302.

Hall CR. (1965). The scattering of high energy electrons by the thermal motions of crystals. Phil. Mag. **12**, 815-826.

Hall CR, Hirsch PB. (1965). Effect of thermal diffuse scattering on propagation of high energy electrons through crystals. Proc. Roy. Soc. A**286**, 158-177.

Høier R. (1973). Multiple scattering and dynamical effects in diffuse electron scattering. Acta Cryst., A**29**, 663-672.

Honjo G, Kodera S, Kitamura N. (1964). Diffuse streak diffraction patterns from single crystals I. General discussion of aspects of electron diffraction diffuse streak pattern. J. Phys. Soc. Japan **19**, 351-367.

Howie A. (1963). Inelastic scattering of electrons by crystals I. The theory of small-angle inelastic scattering. Proc. Roy. Soc. (London) **271**, 268-287.

Humphreys CJ, Whelan MJ. (1969). Inelastic scattering of fast electron by crystals I. Single electron excitations. Phil. Mag. **20**, 165-172.

Inokuti M. (1971). Inelastic collisions of fast charged particles with atoms and molecules-The Bethe theory revised. Rev. Mod. Phys. **43**, 297-347.

Ishizuka K. (1982). Multislice formula for inclined illumination. Acta Cryst. A**38**, 773-779.

Ishizuka K, Uyeda N. (1977). A new theoretical and practical approach to the multislice method. Acta. Cryst. A**33**, 740-749.

Komatsu K, Teramoto K. (1966). Diffuse streak pattern from various crystals in X-ray and electron diffraction. J. Phys. Soc. Japan **21**, 1152-1159.

Krivanek OL, Ahn CC, Wood GJ. (1990). The inelastic contribution to high resolution images of defects. Ultramicroscopy **33**, 177-185.

Loane RF, Xu P, Silcox J. (1991). Thermal vibrations in convergent beam electron diffraction. Acta Cryst. A**47**, 267-278.

Maslen VW, Rossouw CJ. (1984). Implications of (e, 2e) scattering for inelastic electron diffraction in crystals I. Theory. Phil. Mag. **49**, 735-757.

Okamoto K, Ichinokawa T, Ohtsuki Y. (1971). Kikuchi patterns and inelastic scattering. J. Phys. Soc. Japan, **30**, 1690-1700.

Radi G. (1970). Complex lattice potentials in electron diffraction calculated for a number of crystals. Acta Cryst. A**26**, 41-56.

Raether H. (1980). Excitation of plasmons and interband transitions by electrons. Springer tracts in modern physics **88**. Springer-Verlag, New York, 35-44.

Reimer L, Fromm I, Naundorf. (1990). Electron spectroscopic diffraction. Ultramicroscopy **32**, 80-91.

Rez P, Humphreys CJ, Whelan MJ. (1977). The distribution of intensity in electron diffraction patterns due to phonon scattering. Phil. Mag. **35**, 81-96.

Rossouw CJ, Bursill LA. (1985). Interpretation of dynamical diffuse scattering of fast electrons in rutile. Acta Cryst. A**41**, 320-328.

Spence JCH, Spargo AE. (1971). Observation of double-plasmon excitation in aluminum. Phys. Rev. Lett. **26**, 895-897.

Stobbs WM, Saxton WO. (1988). Quantitative high resolution transmission electron microscopy: the need for energy filtering and the advantages of energy-loss imaging. J. Microscopy **151**, 171-184.

Takagi S. (1958). On the temperature diffuse scattering of electrons. I. Deviations of general formulae. J. Phys. Soc. Jpn. **13**, 278-286.

Tang D, Brydson RD, Jefferson DA, Thomas JM. (1989). The effects of adsorption and inelastic scattering of high-resolution electron microscopic images of $YBa_2Cu_3O_{7-x}$.

Wang ZL. (1992a). Dynamics of thermal diffuse scattering in high-energy electron diffraction and imaging: theory and experiments. Phil. Mag. B**65**, 559-587.

Wang ZL. (1992b). Dynamical simulations of energy-filtered inelastic electron diffraction patterns. Acta Cryst. A**48**, 674-688.

Wang ZL. (1991) Multiple-inelastic scattering in high-energy electron diffraction and imaging. Acta Cryst. A**47**, 686-698.

Wang ZL. (1990). Dynamical inelastic scattering in high-energy electron diffraction and imaging: a new theoretical approach. Phys. Rev. B **41**, 12818-12837.

Wang ZL. (1989). A multislice theory of electron inelastic scattering in a solid. Acta. Cryst. A**45**, 636-645.

Wang ZL, Bentley J. (1991a). Theory of phase correlations in localized inelastic electron diffraction and imaging. Ultramicroscopy, **38**, 181-213.

Wang ZL, Bentley J. (1991b). Energy-filtered HREM images of valence-loss electrons. Microscopy Microstructure Microanalysis **2**, 301-314.

Wang ZL, Bentley J. (1991c). Valence and phonon excitations in high-resolution electron microscopy. Inst. Phys. Conf. Ser. No 119, 547-550.

Wang ZL, Cowley JM. (1990). Dynamic theory of high-angle annular-dark-field STEM lattice images for Ge/Si interfaces. Ultramicroscopy **32**, 275-289.

Whelan MJ. (1965a). Inelastic scattering of fast electrons by crystals. I. interband excitations. J. Appl. Phys. **36**, 2099-2102.

Whelan MJ. (1965b). Inelastic scattering of fast electrons by crystals. II. Phonon scattering. J. Appl. Phys. **36**, 2103-2110.

Yoshioka H. (1957). Effect of inelastic waves on electron diffraction. J. Phys. Soc. Jpn. **12**, 618-628.

Discussion with Reviewers

D. Van Dyck: In order to derive Eq. (4a) one has neglected the $\nabla^2\phi_n$ term, can this term becomes important for localized inelastic scattering?

Authors: Neglecting the $\nabla^2\phi_n$ term significantly simplifies the mathematical operation. The wave function solution (Eq. (7)) under this approximation is equivalent to the inelastic multislice theory (see Appendix A). It is important to note that the multislice solution of Eq. (1) (Eq. (A.11) in Appendix A) was derived without neglecting the $\nabla^2\phi_n$ term and with no assumption on the localized nature of the inelastic scattering event (Wang, 1989). This means that the approximation, $\nabla^2\phi_n\Psi_n^0 << 2\nabla\phi_n \bullet \nabla\Psi_n^0$, is valid for localized and delocalized inelastic scattering, and so is Eq. (4a).

K. Ishizuka: To derive the basic equation, Eq. (7), you have assumed a thin crystal with no absorption effects of the inelastic scattering. Would you show us a rough idea on the maximum specimen thickness for each inelastic events.

Authors: Equation (7) was derived based on the single inelastic scattering approximation witnout considering absorption. In practice, the inelastic absorption effect can be effectively included in the calculation of the elastic wave with the use of a complex crystal potential in Eq. (3). The crystal thickness up to which the single inelastic scattering model holds is determined primarily by the scattering cross-section of each process.

If multiple-inelastic scattering for a single process can be described by the Poisson distribution law, the intensity ratio of double-inelastic to single inelastic scattering is $d/2\Lambda$, where Λ is the mean-free-path (MFP) of the inelastic scattering process. Therefore, the single inelastic scattering model is considered a good approximation if $d/\Lambda < 0.5$.

For plasmon excitations at 100 kV, $\Lambda_p \approx 100$ nm for Al (Raether, 1980). The single plasmon excitation model should be adequate for specimen thicknesses less than ~ 50 nm.

For TDS, the MFP depends strongly on the atomic number Z. Calculations for 100 kV electrons at T = 300 K have shown $\Lambda_{TDS} \approx 340$ nm for Al (Hall and Hirsch, 1965). Therefore, for Al and Si, the single phonon scattering model is valid if $d < 150$ nm. For high Z elements Λ_{TDS} may be considerably small.

For core-shell excitations, since the atomic ionization cross-section is extremely small, the single inner-shell scattering model is always an excellent approximation for normal TEM specimens. However, for $d > \Lambda_p/2$, inner shell - plasmon multiple scattering becomes important.